Science Signaling
AAAS

` The Mammalian MAPK/ERK Pathway Exhibits Properties of a Negative Feedback Amplifier

Oliver E. Sturm, Richard Orton, Joan Grindlay, Marc Birtwistle, Vladislav Vyshemirsky, David Gilbert, Muffy Calder, Andrew Pitt, Boris Kholodenko and Walter Kolch (21 December 2010)
Science Signaling **3** (153), ra90. [DOI: 10.1126/scisignal.2001212]

Science Signaling (ISSN 1937-9145) is published weekly, except the last week in December, by the American Association for the Advancement of Science, 1200 New York Avenue, NW, Washington, DC 20005.

COMPUTATIONAL BIOLOGY

The Mammalian MAPK/ERK Pathway Exhibits Properties of a Negative Feedback Amplifier

Oliver E. Sturm,[1*†] Richard Orton,[1*‡] Joan Grindlay,[2*] Marc Birtwistle,[3] Vladislav Vyshemirsky,[1§] David Gilbert,[1‖] Muffy Calder,[1] Andrew Pitt,[4] Boris Kholodenko,[3] Walter Kolch[3,5¶]

(Published 21 December 2010; Volume 3 Issue 153 ra90)

Three-tiered kinase modules, such as the Raf–MEK (mitogen-activated or extracellular signal–regulated protein kinase kinase)–ERK (extracellular signal–regulated kinase) mitogen-activated protein kinase pathway, are widespread in biology, suggesting that this structure conveys evolutionarily advantageous properties. We show that the three-tiered kinase amplifier module combined with negative feedback recapitulates the design principles of a negative feedback amplifier (NFA), which is used in electronic circuits to confer robustness, output stabilization, and linearization of nonlinear signal amplification. We used mathematical modeling and experimental validation to demonstrate that the ERK pathway has properties of an NFA that (i) converts intrinsic switch-like activation kinetics into graded linear responses, (ii) conveys robustness to changes in rates of reactions within the NFA module, and (iii) stabilizes outputs in response to drug-induced perturbations of the amplifier. These properties determine biological behavior, including activation kinetics and the response to drugs.

INTRODUCTION

Three-tiered kinase modules are a common motif in signal transduction pathways that enable precise cellular responses to extracellular cues. The prototypic mitogen-activated protein kinase (MAPK) cascades consist of a guanosine triphosphatase (GTPase)–regulated initial kinase [MAPK kinase kinase (MAPKKK)], which phosphorylates and activates an intermediate kinase (MAPKK) with narrow substrate specificity that phosphorylates and activates the third kinase (MAPK), which is the main pathway effector and usually has multiple substrates (*1*). The biological reason for this design is unclear. Theoretical considerations suggest that it enables high signaling rates and amplification while providing stable off states (*2*). Negative feedback loops (NFLs) are predicted to add rich dynamic properties to signaling pathways, such as oscillations and switch-like responses (*3*). In metabolic pathways, NFLs stabilize end-product concentrations with respect to changes in consumption rates or substrate input supplies (*4*). Combining experimental and mathematical analysis, we show that the integration of a kinase cascade amplifier with NFLs generates emergent system-level properties that resemble the negative feedback amplifier (NFA) known from engineering, and that these NFA-like properties affect drug sensitivity and adaptation to perturbations of cells. We analyzed the extracellular signal–regulated kinase (ERK) MAPK pathway, which regulates fundamental cellular processes including proliferation, survival, transformation, differentiation, and motility (*5*, *6*). ERK signaling is initiated by cell surface receptors that activate Ras by recruiting guanine nucleotide exchange factors, such as SOS, which load Ras with guanosine triphosphate (GTP) (*5*, *7*, *8*). RasGTP binds MAPKKKs of the Raf family with high affinity, translocating them from the cytosol to the cell membrane where they become activated. Active Raf phosphorylates and activates mitogen-activated or extracellular signal–regulated protein kinase kinase (MEK), which in turn phosphorylates and activates ERK.

[1]Department of Computing Science, University of Glasgow, Glasgow G12 8QQ, UK. [2]Signalling and Proteomics Laboratory, Beatson Institute for Cancer Research, Garscube Estate, Switchback Road, Glasgow G61 1BD, UK. [3]Systems Biology Ireland, University College Dublin, Belfield, Dublin 4, Ireland. [4]Sir Henry Wellcome Functional Genomics Facility, University of Glasgow, Glasgow G12 8QQ, UK. [5]Conway Institute, University College Dublin, Belfield, Dublin 4, Ireland.
*These authors contributed equally to this work.
†Present address: Department of Immunology, St. Jude Children's Research Hospital, Memphis, TN 38104, USA.
‡Present address: Comparative Epidemiology Group, Faculty of Veterinary Medicine, University of Glasgow, Glasgow G61 1QH, UK.
§Present address: Department of Mathematics and Statistics, University of Strathclyde, Glasgow G1 1XH, UK.
‖Present address: School of Information Systems, Computing and Mathematics, Brunel University, Uxbridge, Middlesex UB8 3PH, UK.
¶To whom correspondence should be addressed. E-mail: walter.kolch@ucd.ie

RESULTS

The NFA design and experimental approaches to examine NFA-like properties of the Raf-MEK-ERK pathway

In engineering, the NFA design (Fig. 1A) is widely used for controlling dynamic processes to reduce the effects of input noise, buffer perturbations in the amplifier, and smoothen output responses (*9*, *10*). In a Raf-MEK-ERK biological circuit, the input signal coming from receptors proceeds through activated RasGTP to the amplifier, represented by the Raf-MEK-ERK module (Fig. 1B). The ratio of protein abundances of Raf-1, MEK, and ERK is about 1:3:6 in COS cells and 1:0.7:9 in NIH 3T3 fibroblasts (fig. S1), thus permitting signal amplification. A direct NFL from ERK to SOS, involving its phosphorylation and inhibition (*11*), inhibits Ras activation, and another NFL involves Raf-1 phosphorylation and inhibition (*12*) by activated ERK. A key property of an NFA is to convey robustness against perturbations to the amplifier (Fig. 1C), while still linearly transmitting input signals (Fig. 1D). To explore the NFA properties of the ERK pathway, we modeled it as either a simple amplifier ("Feedback Broken") or an NFA ("Feedback Intact"), using ordinary differential equations (Supplementary Materials, sections 1.1 and 1.2, and fig. S2). The Feedback Intact model starts with Ras as the input reflecting Raf stimulation by different growth factors and ends with ERK activity, as measured by ERK phosphorylation, as output. To test the predictions of this model experimentally, we used two strategies to eliminate the NFLs (Fig. 1E and fig. S3). Introduction of Raf6A, a Raf-1 mutant

where all six ERK phosphorylation sites are replaced by alanines (*12*), eliminated the feedback from ERK to Raf6A, but not the feedback to SOS or to endogenous Raf-1. Both feedback loops were eliminated if the pathway was activated by BXB-ER, which consists of the kinase domain of Raf-1 (BXB) fused to the hormone-binding domain of the estrogen receptor (ER) (*13*). The kinase activity of BXB-ER is directly activated by 4-hydroxy-tamoxifen (4HT), bypassing growth factor receptors and Ras proteins (*13*). BXB-ER lacks five of the six ERK phosphorylation sites, rendering it resistant to negative ERK feedback regulation. To ensure that the results were directly comparable, we calibrated (i) the mathematical model to provide equal input strengths through Raf-1 activated by RasGTP and BXB-ER activated by 4HT (Supplementary Materials, section 1.3), leaving the other parameters the same; and (ii) the biological system by titrating 4HT to adjust the kinase activity of BXB-ER to that of endogenous Raf-1 activated by epidermal growth factor (EGF)–stimulated RasGTP accumulation (Fig. 1F), and by expressing Raf6A at similar abundance as a wild-type Raf-1 control (fig. S4). Exposure of EGF- or 4HT-stimulated cells to the MEK inhibitor U0126 (*14*, *15*) had no effect on BXB-ER activity, but prolonged the activity of Raf-1. Cells expressing Raf6A had slightly increased basal kinase activity, which was stimulated by EGF but, in contrast to Raf-1, was sustained even in the absence of U0126 (Fig. 1F). These results showed that the negative feedback limits the duration of Raf-1 activation and that our experimental tools are suitable to interrogate the NFA design.

Conversion of switch-like ERK activation into a graded response by the NFA-like design

In the ERK pathway, amplifier distortions arise naturally because MEK phosphorylates each of the two sites required for full ERK activity separately rather than processively during one binding event (*16*, *17*). As a result, the single-phosphorylated, low-activity form of ERK is generated during the initial activation phase. When enough single-phosphorylated ERK has accumulated, every new phosphorylation event produces double-phosphorylated, fully activated ERK, which is apparent as a steep nonlinear increase in ERK activation kinetics (*18*). This hypersensitive mode of activation changes the internal gain of the amplifier in a nonlinear fashion, resulting in a switch-like response, which is predicted by our mathematical model (Fig. 2A), and was observed experimentally in *Xenopus* oocytes

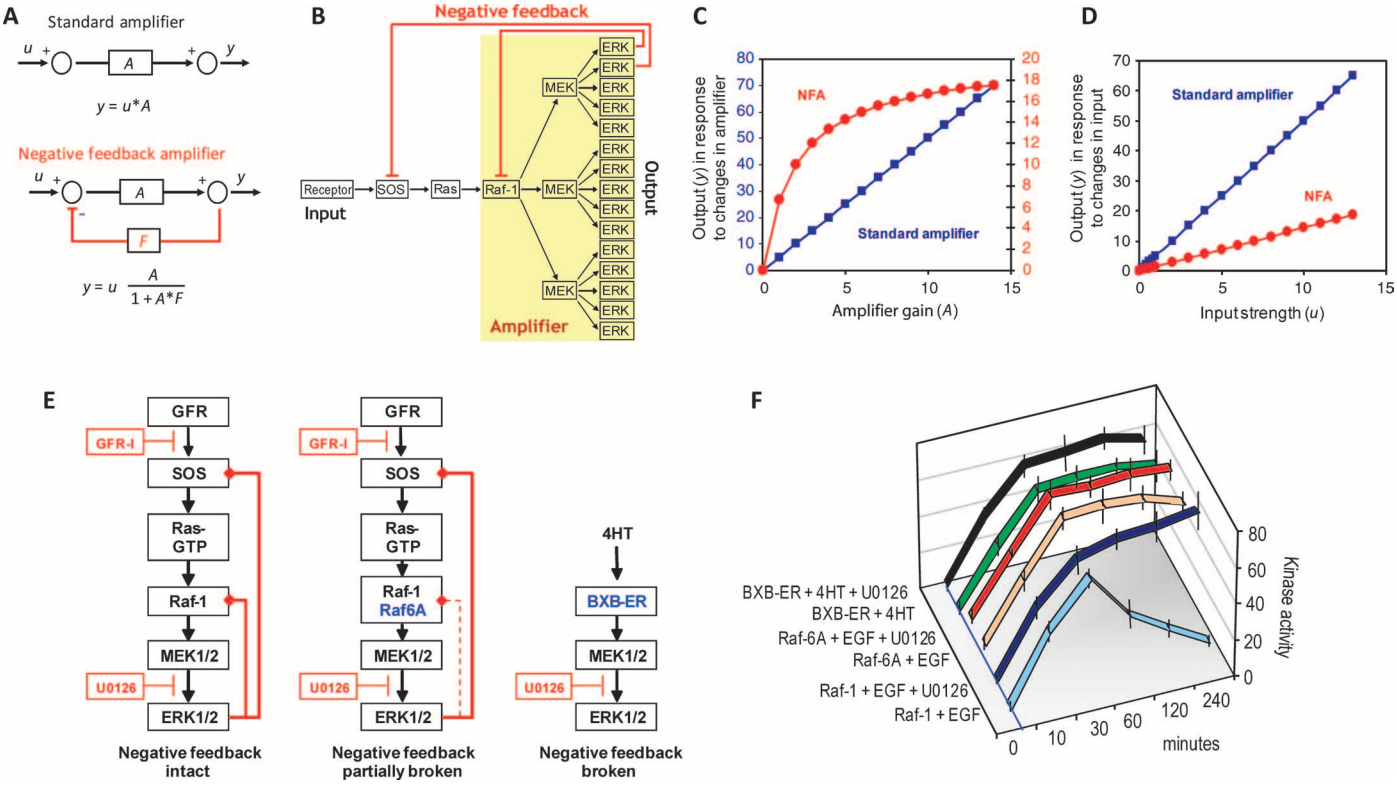

Fig. 1. The ERK pathway resembles a negative feedback amplifier (NFA). (**A**) Blueprint of a standard amplifier and an NFA; *u* = input; *y* = output; *A* = amplification; *F* = feedback. (**B**) The ERK pathway resembles an NFA with an amplifier consisting of the three-tiered kinase module Raf-MEK-ERK and feedbacks emanating from ERK to SOS and Raf-1 activation. (**C**) Simulation of signal input-output relationships (*u*/*y*) in regard to changes in the amplifier (amplification strength, *A*) for a standard amplifier (blue line and blue *y*-axis labels) and an NFA (red line and red *y*-axis labels). (**D**) Simulation of signal input-output relationships in regard to changes in input (*u*) signals in a standard amplifier (blue line) and an NFA (red line). (**E**) Strategies to break the NFA. GFR, growth factor receptor; GFR-I, GFR inhibitors; U0126, MEK inhibitor; solid red lines ending in diamonds represent negative feedback interactions; dashed red lines ending in diamonds indicate partial loss of negative feedback; blue molecules indicate introduced mutant or fusion proteins. (**F**) Kinase activities of Raf-1 and Raf-1 mutants. Flag-tagged Raf-1 and Raf6A or HA-tagged BXB-ER was expressed in COS1 cells. Serum-starved cells were treated with 10 μM U0126 before stimulation with EGF (50 ng/ml) or 0.1 μM 4HT. At the indicated time points, tagged Raf proteins were immunoprecipitated and assayed for kinase activity. Error bars represent SEM (*n* = 4).

(*19*). According to our mathematical NFA model simulations (Fig. 2A), the negative feedback should convert the switch-like, hypersensitive response into a more graded response by reducing the sensitivity of the reactions in the amplifier module to perturbations (Fig. 2A). To test this prediction theoretically, we performed sensitivity analysis of the mathematical model (Fig. 2B and Supplementary Materials, section 1.5). Sensitivity coefficients provide a quantitative measurement of how changes in individual reactions affect the output, here measured as the abundance of doubly phosphorylated ERK (ppERK). Elimination of the negative feedback increased the sensitivity coefficients of most reactions in the amplifier module, especially the reactions that activate and deactivate MEK. This increase in the sensitivity coefficients in the amplifier module is explained by the mathematical model because the strength of the negative feedback is directly coupled to the gain of the amplifier, which corrects variations in the parameters in the amplifier module. Thus, the biological NFA allowed signal amplification but made the system resilient to amplifier perturbations.

The theoretical analysis of the NFA model predicted that ERK activation should be switch-like in the absence of negative feedback, but graded when it is present. To test this prediction experimentally, we analyzed ERK activation by flow cytometry, which measures ERK activity in individual cells of a population (Fig. 2C). In the Feedback Intact system, ERK activation increased in a graded manner proportional to the stimulation. However, in the Feedback Broken system, the response be-

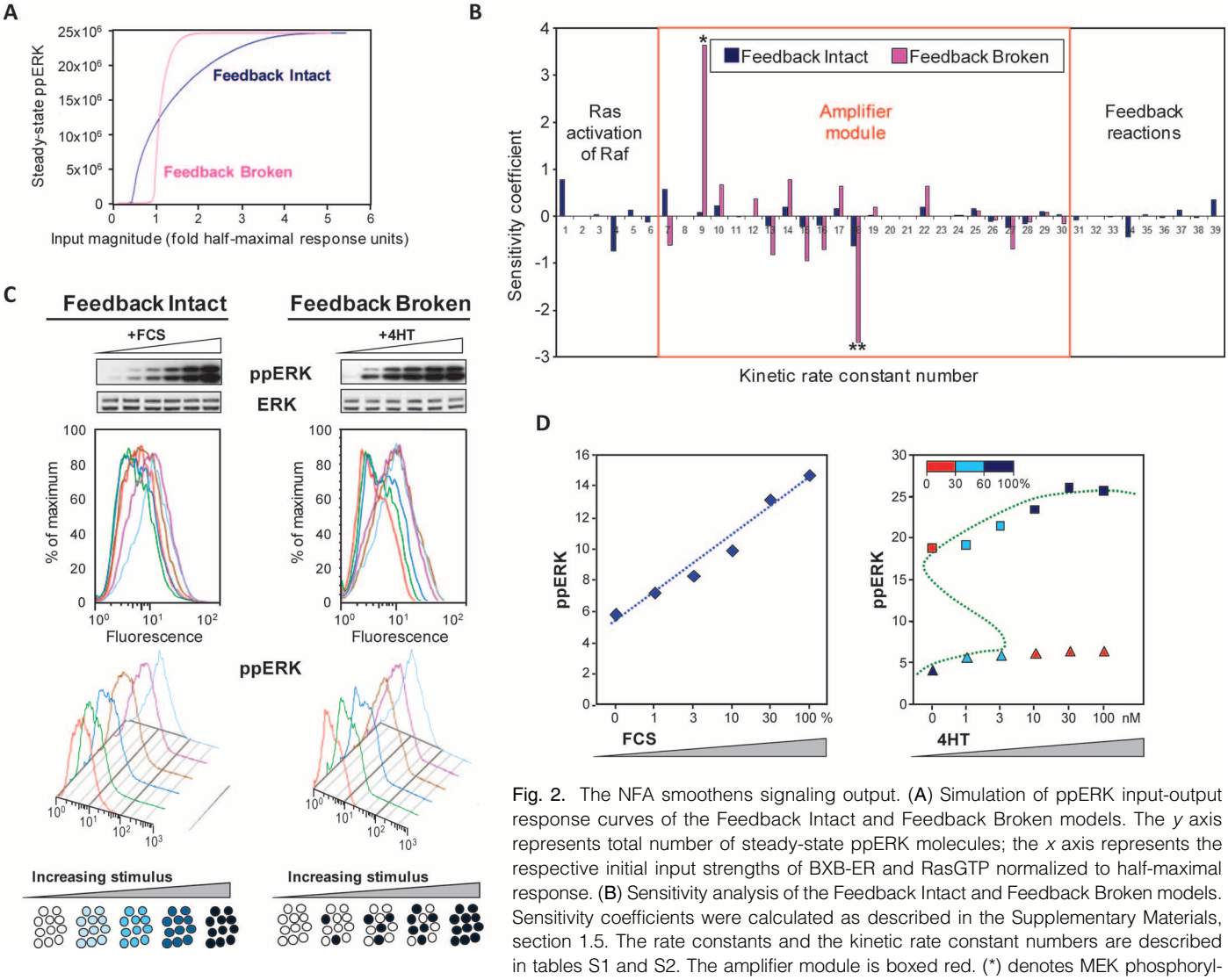

Fig. 2. The NFA smoothens signaling output. (**A**) Simulation of ppERK input-output response curves of the Feedback Intact and Feedback Broken models. The *y* axis represents total number of steady-state ppERK molecules; the *x* axis represents the respective initial input strengths of BXB-ER and RasGTP normalized to half-maximal response. (**B**) Sensitivity analysis of the Feedback Intact and Feedback Broken models. Sensitivity coefficients were calculated as described in the Supplementary Materials, section 1.5. The rate constants and the kinetic rate constant numbers are described in tables S1 and S2. The amplifier module is boxed red. (*) denotes MEK phosphorylation by Raf-1; (**) denotes MEK dephosphorylation. (**C**) NFA effects on ERK activation kinetics. NIH 3T3 cells stably expressing BXB-ER (*31*) were stimulated with increasing amounts of 4HT (0, 1, 3, 10, 30, and 100 nM) or fetal calf serum (FCS; 0, 1, 3, 10, 30, and 100%) for 20 min. ERK phosphorylation (ppERK) was determined by Western blotting and flow cytometry analysis. The data are representative of three independent experiments, in each of which 10^5 cells were analyzed. The schematic at the bottom illustrates the interpretation of the data. (**D**) Means of the ppERK fluorescence intensity distributions from (C) are plotted as a function of FCS or 4HT concentration. Triangles and squares represent the first and second peaks in the bimodal 4HT distribution, respectively. The color bar represents the percentage of cells in each category.

came switch-like, in which individual cells either responded or not, and the number of responding cells increased in proportion to the stimulation. Thus, the presence or absence of the NFLs can determine whether the response of the kinase module is graded or switch-like (Fig. 2D). This may explain divergent results about the activation kinetics of the ERK cascade in different biological systems. Although it has switch-like properties in *Xenopus* oocytes (*19*), subsequent studies in mammalian cells found that it responded in a graded fashion (*20*, *21*). In *Xenopus* oocytes, the main mitotic activator of the ERK module is not Raf-1 but c-Mos (*22*). c-Mos lacks the Ras-binding domain and the ERK phosphorylation sites, and hence is not subjected to negative feedback regulation by ERK, resulting in switch-like ERK activation dynamics. However, in mammalian cells in which Raf-1 activates MEK, growth factor stimulation permits the NFA properties to buffer the intrinsic hypersensitivity of the amplifier and generate a graded response.

The NFA-like design and drug sensitivity

Another salient prediction of the NFA model is that ERK activation should be resilient to disturbances of the amplifier (Fig. 1C). To test this prediction, we used the MEK-selective inhibitor U0126 (*14*, *15*). Computational simulations of U0126 dose-response curves predicted high sensitivity of ERK activation to MEK inhibition in the absence of NFLs (Feedback Broken) and resistance to MEK inhibition in the presence of the NFA (Feedback Intact) (Fig. 3A). To test this prediction, we treated cells having the negative feedback either intact or broken with varying amounts of the MEK-selective inhibitor U0126, stimulated them with either EGF (Feedback Intact) or 4HT (Feedback Broken), and then measured ERK activation (*14*, *15*). As predicted by our model, in the Feedback Broken system, ERK activation was thoroughly inhibited by low concentrations of U0126, whereas in the Feedback Intact system, ERK activity persisted even in the presence of high U0126 concentrations (Fig. 3B). With the negative feedback intact, increasing U0126 concentrations weakened the negative feedback and allowed the amplifier gain to rise, thus causing increased resistance to U0126. As inhibitor concentrations were increased further, resistance persisted until U0126 concentrations were high enough to achieve complete inhibition.

We also observed enhanced sensitivity to low U0126 concentrations in the Feedback Intact system. This effect can be explained by three mechanisms, which can operate separately or jointly depending on conditions and inhibitor properties. First, low inhibitor concentrations are inherently associated with linear inhibition kinetics that precede the flattening out of the inhibition curve when rising inhibitor concentrations push the system toward saturation. Linear inhibition ranges are generally larger for tightly bound inhibitors, such as U0126 (*15*). Second, the allosteric mode of inhibition by U0126 fixes MEK in a nonfunctional conformation and prevents MEK from interacting with ERK (*23*). Thus, U0126 not only prevents MEK from binding to ERK but also disrupts MEK-ERK complexes (reactions 27 to 35 in table S1), making inhibition more efficient. Third, if the concentration of ppERK is larger than the abundance of the upstream activator Raf-1 (fig. S1), the negative feedback becomes saturated. In this last scenario, a large reduction of ppERK would be required before Raf-1 inhibition eased and the feedback weakened to allow the increase of input to compensate for the inhibition.

The sensitivities to MEK inhibition that we observed in the computational simulations were obtained with the parameter values from the model by Schoeberl *et al*. (*24*). To test whether variations in the concentrations of Raf-1, MEK, and ERK affected the model, we used the concentrations determined in COS1 cells (fig. S1). The results showed that the effects of MEK inhibition in the Feedback Intact and Feedback Broken models (fig. S5) were similar to those in the simulations in Fig. 3B. In conjunction with the experiments shown in Fig. 2, C and D, where we enhanced the activity of the amplifier module, the inhibition experiments shown in Fig. 3, A and B, demonstrated that the NFA-like design of the ERK pathway conveyed resistance to perturbations of the amplifier caused by increasing concentrations of the MEK inhibitor. These results also showed that the biological circuit is more complex than the classic electronic circuit. One main difference is the temporal element of feedback regulation, which is immediate in the classic electronic NFA, but can be delayed or operating on different parallel time scales in the biological design. Because the effects of U0126 included parallel effects that can occur on different time scales, we tested a situation where U0126 was applied at the peak of ERK activation (fig. S6). In the Feedback Broken system, U0126 caused full ERK inhibition, whereas the Feedback Intact system exhibited dampened inhibition, resulting in a partial recovery to a new steady state of ERK activity above the basal activity. These results suggest that the NFA-like design of biological systems can dynamically buffer amplifier perturbations over time.

The model also predicts that inhibition of components that are not part of the biological NFA should be more effective than inhibition of components within the NFA (Fig. 3A). This prediction was corroborated by comparing the effects of 4557W, an EGF receptor (EGFR) inhibitor, with that of U0126 (Fig. 3B). Inhibition of EGFR produced an almost linear dose-response relationship both in the model and in the experimental system. This suggests that proteins embedded in NFA-like topologies make suboptimal drug targets, because the effects of their inhibition are dampened.

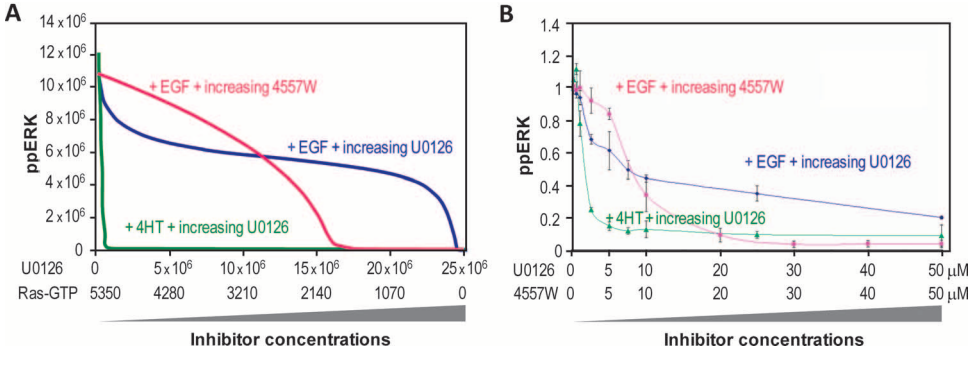

Fig. 3. The NFA-like property determines the responses of the ERK pathway to drugs that inhibit different components of the pathway. (A) Predicted sensitivity profiles to MEK (U0126) and EGFR (4775W) inhibitors. The *y* axis represents numbers of ppERK molecules. U0126 was modeled as an allosteric inhibitor, and concentrations are given as number of molecules. The effects of 4775W were modeled as a decrease in the number of RasGTP molecules. (B) Measured sensitivity profiles to U0126 and 4775W inhibitors. COS1 cells stably expressing BXB-ER cells were treated with U0126 or 4775W for 1 hour and subsequently stimulated with EGF or 4HT for 20 min. The *x* axis shows inhibitor concentrations, and the *y* axis arbitrary response units based on quantitative LI-COR analysis of Western blot measurements of phosphorylated ERK (ppERK). Data represent the average of three experiments; error bars are SD.

We also tested the effects of the biological NFA with the "Feedback Partially Broken" system based on the Raf6A mutant (*12*) to partially break the negative feedback. Unfortunately, due to cytotoxic effects, we could not obtain cells expressing Raf6A alone in the absence of endogenous Raf-1. Therefore, we used COS1 cells stably expressing similar amounts of Raf-1 or Raf6A (fig. S4). These cells were stimulated with EGF and treated with increasing doses of U0126. In response to EGF stimulation, cells expressing Raf6A were more sensitive to MEK inhibition than were cells expressing Raf-1 (Fig. 4A, upper left). To examine the specificity of the NFA-like effect, we tested different growth factors, in particular platelet-derived growth factor (PDGF) and insulin-like growth factor 1 (IGF-1), factors for which COS1 cells have receptors. PDGF-activated ERK showed an NFA-like response that was similar but smaller than the response to EGF, with cells expressing Raf6A showing decreased resistance to U0126 (Fig. 4A, upper right) but not to a PDGF receptor inhibitor (Fig. 4A, lower left), compared to cells expressing Raf-1. The smaller NFA-like effect seen with the inhibitor of the NFA component MEK can be explained by the lesser ability of PDGF to activate ERK (fig. S7), which weakens the influence of the NFA (Fig. 1A). Curiously, stimulation of ERK by IGF-1 did not exhibit the NFA-like property that partial loss of negative feedback made the MEK inhibitor more effective in reducing ERK activation (Fig. 4A, lower right). We found that IGF-1 selectively activated B-Raf and not Raf-1 (Fig. 4B). Although ERK can phosphorylate B-Raf and induce the disassembly of B-Raf–Raf-1 heterodimers at late time points, acute B-Raf activation is not inhibited by ERK (*25*) (fig. S8). Hence, IGF-1–induced ERK activation is not protected from U0126 inhibition by the NFA-like effect from ERK to Raf-1: This feedback may not exist because IGF-1 does not activate Raf-1, or if B-Raf signaling leading to ERK activation does result in ERK phosphorylation of Raf-1, then this phosphorylation will have no consequences for IGF-1 responses. These results suggest that the NFA model applies to ERK activated downstream of Raf-1, but not B-Raf, which is consistent with the observation that cancer cells harboring mutated B-Raf are highly susceptible to MEK inhibitors (*26*, *27*). The susceptibility of cancers with B-Raf mutations to MEK inhibitors may be due to the lack of negative feedback buffering of MEK inhibition, leading to effective inhibition of ERK activation. Results demonstrating a switching from B-Raf to Raf-1 as the main activator of the ERK pathway in melanoma (*28*) highlight the possibility that this switch could be accompanied by increased resistance to MEK inhibitors due to the acquisition of NFA-like properties. Our results predict that breaking the NFA is essential to ensure sensitivity to MEK inhibitors.

Therefore, we used our model to suggest scenarios for disabling the biological NFA. One possibility is to inhibit targets outside of the biological NFA (Figs. 3, A and B, and 4A). An alternative prediction of the mathematical NFA model was that Raf-1 inhibition should sensitize the pathway to MEK inhibition by weakening the NFA effect (Fig. 5A). This prediction seems counterintuitive because Raf-1–MEK–ERK is a linear activation cascade. However, as predicted by the NFA model, the Raf-1 inhibitor GW5074 increased the sensitivity to MEK inhibition in the Feedback Intact system (Fig. 5B, left). The cooperative effects of Raf and MEK inhibition were absent in the Feedback Broken system (Fig. 5B, right).

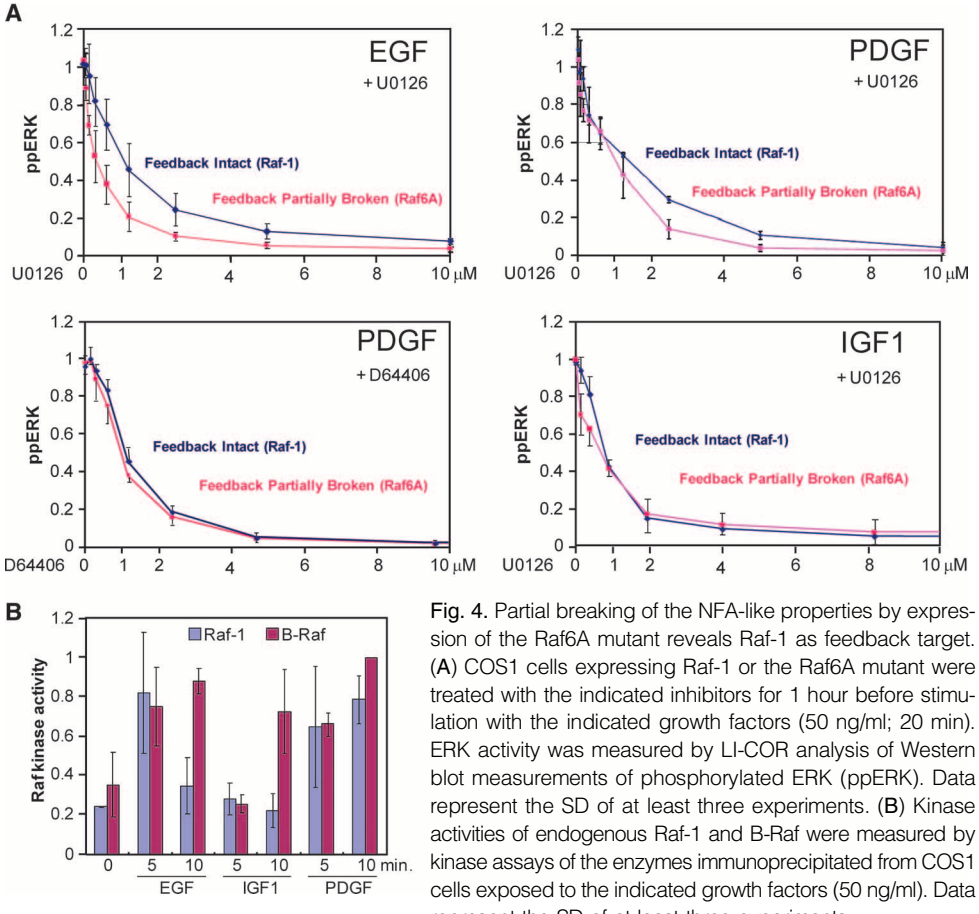

Fig. 4. Partial breaking of the NFA-like properties by expression of the Raf6A mutant reveals Raf-1 as feedback target. (**A**) COS1 cells expressing Raf-1 or the Raf6A mutant were treated with the indicated inhibitors for 1 hour before stimulation with the indicated growth factors (50 ng/ml; 20 min). ERK activity was measured by LI-COR analysis of Western blot measurements of phosphorylated ERK (ppERK). Data represent the SD of at least three experiments. (**B**) Kinase activities of endogenous Raf-1 and B-Raf were measured by kinase assays of the enzymes immunoprecipitated from COS1 cells exposed to the indicated growth factors (50 ng/ml). Data represent the SD of at least three experiments.

DISCUSSION

These results suggest that the ERK pathway has intrinsic design features like that of an NFA. Although the biological circuitry differs from the engineering blueprint by its greater complexity and nonlinearity, it conveys salient NFA properties including graded response characteristics, robustness to change, and output stabilization. These have important implications for the regulation of the pathway and the design of inhibitors. For instance, the presence of the negative feedback dictates whether ERK activation follows a graded or a switch-like pattern, as demonstrated by the differences in ERK activation responses when the negative feedback is broken (Fig. 2, B to D). Thus, the biological NFA provides a mechanism to generate analog or digital responses. Another implication is in the choice of targets for pharmacological intervention. Signal transduction pathways are important drug targets (*29*, *30*). However, it has proven difficult to predict which components should be targeted, and the cornucopia of potential drug targets is contrasted by a paucity of objective criteria for how to choose

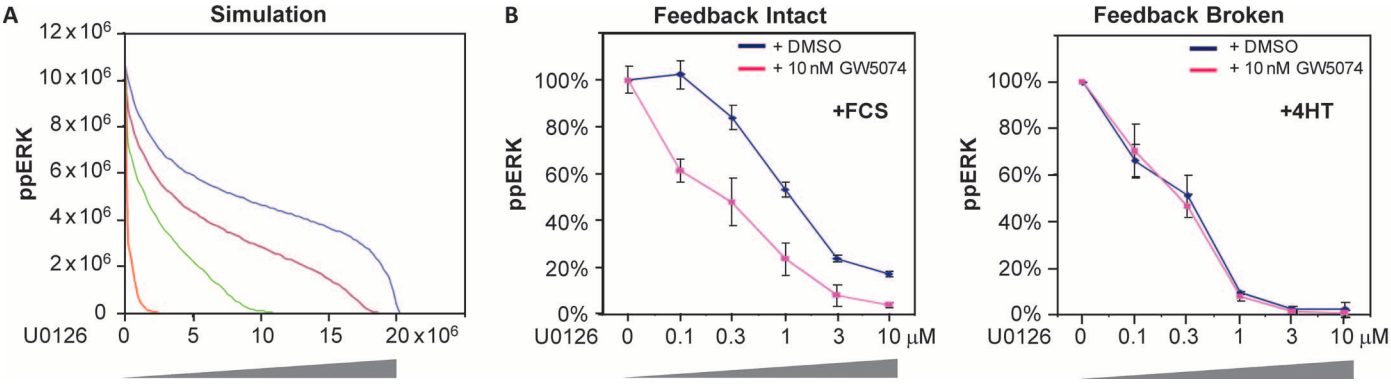

Fig. 5. Cooperation between Raf and MEK inhibitors. (**A**) Model predictions of ppERK abundance at different combinations of Raf (GW5074) and MEK (U0126) inhibitors. The *y* and *x* axes show numbers of ppERK and U0126 molecules, respectively. (**B**) Serum-starved NIH 3T3 BXB-ER cells (*31*) were treated with 10 nM Raf-1 inhibitor (GW5074) and various amounts of the MEK inhibitor U0126 for 60 min and then stimulated with 10% FCS or 100 nM 4HT for 15 min. ppERK was measured by quantitative LI-COR analysis of Western blot measurements of phosphorylated ERK. Error bars represent the SD from the mean of triplicate points.

among them. Our results suggest that inhibition of a pathway by inhibiting targets embedded in an NFA-like topology is more difficult to achieve than the effect of inhibiting targets outside of the feedback loop, which provides a simple drug target selection guideline that is deductible from the network structure. The NFA-like properties also suggest that drugs that inhibit targets within the NFA circuit may be more effective if the NFLs are also blocked or inhibited, thus providing insight into potentially effective combination therapies. On a more speculative note, the results also suggest that biological evolution and engineered systems may converge to similar solutions when designing robustness.

MATERIALS AND METHODS

Reagents and plasmids

Growth factors, drugs, and pharmacological inhibitors were from commercial sources and used according to suppliers' recommendations or as indicated. Antibodies that recognize phosphorylated ERK1 and 2 (ERK1/2) and antibodies that recognize ERK1/2 for immunoblotting were purchased from Cell Signaling. Antibodies that recognize C-Raf-1 and antibodies that recognize hemagglutinin (HA) for immunoprecipitation were purchased from BD Biosciences and Roche, respectively.

Cell culture

Stable BXB-ER NIH 3T3 cells were described (*31*), and COS1 cell lines stably expressing BXB-ER were generated similarly.

Dose-response curves

BXB-ER COS1, NIH 3T3 wild-type-Raf-1, or NIH 3T3 6A-Raf-1 cells were starved in serum-free medium overnight. The cells were preincubated with the indicated amounts of inhibitors U0126, 4557W, or D-64406 for 1 hour and subsequently stimulated with growth factors (50 ng/ml) or 0.1 μM 4HT. The stimulation was stopped by washing the cells with ice-cold phosphate-buffered saline and immediate freezing at −80°C.

Immunoprecipitation, immunoblotting, and immunocomplex kinase assays

Cells were treated with growth factors with or without inhibitors as indicated and lysed in 25 mM Hepes (pH 7.4), 50 mM NaCl, 5 mM EDTA, and 1% Triton X-100 supplemented with protease inhibitor cocktail (Roche) and phosphatase inhibitors (2 mM NaF, 0.2 mM NaP_2O_5, 0.5 mM sodium orthovanadate, and 10 mM β-glycerophosphate). Immunoprecipitations, Western blotting, and kinase assays were performed as described (*25*). Western blots were developed and scanned with LI-COR technology (http://www.licor.com/bio/index.jsp), which is a quantitative technique for staining Western blots based on infrared imaging.

Fluorescence-activated cell sorting

Fluorescence-activated cell sorting (FACS) was performed as described (*32*). Cells were serum-starved for 2 hours, treated as indicated, and stained with Alexa 488–conjugated antibodies against phosphorylated ERK (Invitrogen). Fluorescence profiles were measured on a FACSCalibur (BD Biosciences) with CellQuest Pro software. Distribution profiles were produced with FlowJo software (7.2.2). Data fitting was performed with Microsoft Excel and GraphPad Prism.

Models and modeling

The mathematical models were based on mass action models using ordinary differential equations of an adapted version of the core ERK pathway described in (*24*). Two computational models, Feedback Intact and Feedback Broken, were developed to investigate the NFA characteristics of the ERK pathway. The NFA-like model is the Feedback Intact model. Details are supplied in the Supplementary Materials, section 1.

SUPPLEMENTARY MATERIALS

www.sciencesignaling.org/cgi/content/full/3/153/ra90/DC1
Section 1. Models and modeling.
Section 2. Model parameters.
Section 3. SBML files of the models.
References
Fig. S1. Absolute concentrations of Raf-1, MEK, and ERK in COS1 and NIH 3T3 cells.
Fig. S2. Schematic topologies of the models used.
Fig. S3. Schematic of Raf-1 and the Raf-1 mutants used to probe the NFA hypothesis.
Fig. S4. Expression of Flag-tagged Raf-1 and the Raf6A mutant.
Fig. S5. The effects of U0126 on steady-state ppERK abundance with protein concentrations of COS1 cells.
Fig. S6. The NFA effect also stabilizes non–steady-state dynamic systems.
Fig. S7. Dose-dependent ERK activation by different stimuli.
Fig. S8. B-Raf kinase activity is not feedback-inhibited by ERK.
Tables S1 to S3. Model parameters (Excel).
SBML files of the models (XML).

REFERENCES AND NOTES

1. M. Raman, W. Chen, M. H. Cobb, Differential regulation and properties of MAPKs. *Oncogene* **26**, 3100–3112 (2007).
2. R. Heinrich, B. G. Neel, T. A. Rapoport, Mathematical models of protein kinase signal transduction. *Mol. Cell* **9**, 957–970 (2002).
3. H. M. Sauro, B. N. Kholodenko, Quantitative analysis of signaling networks. *Prog. Biophys. Mol. Biol.* **86**, 5–43 (2004).
4. M. A. Savageau, *Biochemical Systems Analysis. A Study of Function and Design in Molecular Biology* (Addison-Wesley Pub. Co., Reading, MA, 1976).
5. W. Kolch, Coordinating ERK/MAPK signalling through scaffolds and inhibitors. *Nat. Rev. Mol. Cell Biol.* **6**, 827–837 (2005).
6. P. J. Roberts, C. J. Der, Targeting the Raf-MEK-ERK mitogen-activated protein kinase cascade for the treatment of cancer. *Oncogene* **26**, 3291–3310 (2007).
7. A. S. Dhillon, A. von Kriegsheim, J. Grindlay, W. Kolch, Phosphatase and feedback regulation of Raf-1 signaling. *Cell Cycle* **6**, 3–7 (2007).
8. C. Wellbrock, M. Karasarides, R. Marais, The RAF proteins take centre stage. *Nat. Rev. Mol. Cell Biol.* **5**, 875–885 (2004).
9. H. S. Black, Stabilized feedback amplifiers. *Bell Syst. Tech. J.* **13**, 1–18 (1934).
10. G. Palumbo, S. Pennisi, *Feedback Amplifiers: Theory and Design* (Kluwer Academic, Boston/Dordrecht/London, 2002).
11. E. Douville, J. Downward, EGF induced SOS phosphorylation in PC12 cells involves P90 RSK-2. *Oncogene* **15**, 373–383 (1997).
12. M. K. Dougherty, J. Muller, D. A. Ritt, M. Zhou, X. Z. Zhou, T. D. Copeland, T. P. Conrads, T. D. Veenstra, K. P. Lu, D. K. Morrison, Regulation of Raf-1 by direct feedback phosphorylation. *Mol. Cell* **17**, 215–224 (2005).
13. M. L. Samuels, M. J. Weber, J. M. Bishop, M. McMahon, Conditional transformation of cells and rapid activation of the mitogen-activated protein kinase cascade by an estradiol-dependent human raf-1 protein kinase. *Mol. Cell. Biol.* **13**, 6241–6252 (1993).
14. S. P. Davies, H. Reddy, M. Caivano, P. Cohen, Specificity and mechanism of action of some commonly used protein kinase inhibitors. *Biochem. J.* **351**, 95–105 (2000).
15. M. F. Favata, K. Y. Horiuchi, E. J. Manos, A. J. Daulerio, D. A. Stradley, W. S. Feeser, D. E. Van Dyk, W. J. Pitts, R. A. Earl, F. Hobbs, R. A. Copeland, R. L. Magolda, P. A. Scherle, J. M. Trzaskos, Identification of a novel inhibitor of mitogen-activated protein kinase kinase. *J. Biol. Chem.* **273**, 18623–18632 (1998).
16. W. R. Burack, T. W. Sturgill, The activating dual phosphorylation of MAPK by MEK is nonprocessive. *Biochemistry* **36**, 5929–5933 (1997).
17. M. Schilling, T. Maiwald, S. Hengl, D. Winter, C. Kreutz, W. Kolch, W. D. Lehmann, J. Timmer, U. Klingmuller, Theoretical and experimental analysis links isoform-specific ERK signalling to cell fate decisions. *Mol. Syst. Biol.* **5**, 334 (2009).
18. N. I. Markevich, J. B. Hoek, B. N. Kholodenko, Signaling switches and bistability arising from multisite phosphorylation in protein kinase cascades. *J. Cell Biol.* **164**, 353–359 (2004).
19. J. E. Ferrell Jr., E. M. Machleder, The biochemical basis of an all-or-none cell fate switch in *Xenopus* oocytes. *Science* **280**, 895–898 (1998).
20. J. P. Mackeigan, L. O. Murphy, C. A. Dimitri, J. Blenis, Graded mitogen-activated protein kinase activity precedes switch-like c-Fos induction in mammalian cells. *Mol. Cell. Biol.* **25**, 4676–4682 (2005).
21. A. Whitehurst, M. H. Cobb, M. A. White, Stimulus-coupled spatial restriction of extracellular signal-regulated kinase 1/2 activity contributes to the specificity of signal-response pathways. *Mol. Cell. Biol.* **24**, 10145–10150 (2004).
22. J. Yue, J. E. Ferrell Jr., Mos mediates the mitotic activation of p42 MAPK in *Xenopus* egg extracts. *Curr. Biol.* **14**, 1581–1586 (2004).
23. W. S. VanScyoc, G. A. Holdgate, J. E. Sullivan, W. H. Ward, Enzyme kinetics and binding studies on inhibitors of MEK protein kinase. *Biochemistry* **47**, 5017–5027 (2008).
24. B. Schoeberl, C. Eichler-Jonsson, E. D. Gilles, G. Muller, Computational modeling of the dynamics of the MAP kinase cascade activated by surface and internalized EGF receptors. *Nat. Biotechnol.* **20**, 370–375 (2002).
25. L. K. Rushworth, A. D. Hindley, E. O'Neill, W. Kolch, Regulation and role of Raf-1/B-Raf heterodimerization. *Mol. Cell. Biol.* **26**, 2262–2272 (2006).
26. C. A. Pratilas, A. J. Hanrahan, E. Halilovic, Y. Persaud, J. Soh, D. Chitale, H. Shigematsu, H. Yamamoto, A. Sawai, M. Janakiraman, B. S. Taylor, W. Pao, S. Toyooka, M. Ladanyi, A. Gazdar, N. Rosen, D. B. Solit, Genetic predictors of MEK dependence in non-small cell lung cancer. *Cancer Res.* **68**, 9375–9383 (2008).
27. D. B. Solit, L. A. Garraway, C. A. Pratilas, A. Sawai, G. Getz, A. Basso, Q. Ye, J. M. Lobo, Y. She, I. Osman, T. R. Golub, J. Sebolt-Leopold, W. R. Sellers, N. Rosen, BRAF mutation predicts sensitivity to MEK inhibition. *Nature* **439**, 358–362 (2006).
28. N. Dumaz, R. Hayward, J. Martin, L. Ogilvie, D. Hedley, J. A. Curtin, B. C. Bastian, C. Springer, R. Marais, In melanoma, *RAS* mutations are accompanied by switching signaling from BRAF to CRAF and disrupted cyclic AMP signaling. *Cancer Res.* **66**, 9483–9491 (2006).
29. A. A. Adjei, E. K. Rowinsky, Novel anticancer agents in clinical development. *Cancer Biol. Ther.* **2**, S5–S15 (2003).
30. J. S. Sebolt-Leopold, J. M. English, Mechanisms of drug inhibition of signalling molecules. *Nature* **441**, 457–462 (2006).
31. J. Lovric, S. Dammeier, A. Kieser, H. Mischak, W. Kolch, Activated raf induces the hyperphosphorylation of stathmin and the reorganization of the microtubule network. *J. Biol. Chem.* **273**, 22848–22855 (1998).
32. S. D. Santos, P. J. Verveer, P. I. Bastiaens, Growth factor-induced MAPK network topology shapes Erk response determining PC-12 cell fate. *Nat. Cell Biol.* **9**, 324–330 (2007).

33. **Acknowledgments:** We thank T. Gilbey for help with the FACS analysis and J. Kamburapola for help with the LI-COR gels. **Funding:** This work was supported by a DTI Beacons Project, Cancer Research UK, Engineering and Physical Sciences Research Council Basic Technology research grant EP/E032745/1, Science Foundation Ireland grant no. 06/CE/B1129, and FP7 Marie Curie fellowship no. 236758 to M.B. **Author contributions:** O.E.S., J.G., and A.P. performed the experiments; R.O., V.V., and M.B. did the mathematical modeling; W.K., B.K., M.C., and D.G. designed the study; and W.K., R.O., and M.B. wrote the manuscript. **Competing interests:** The authors declare that they have no competing interests.

Submitted 24 May 2010
Accepted 3 December 2010
Final Publication 21 December 2010
10.1126/scisignal.2001212
Citation: O. E. Sturm, R. Orton, J. Grindlay, M. Birtwistle, V. Vyshemirsky, D. Gilbert, M. Calder, A. Pitt, B. Kholodenko, W. Kolch, The mammalian MAPK/ERK pathway exhibits properties of a negative feedback amplifier. *Sci. Signal.* **3**, ra90 (2010).

Science Signaling
AAAS
www.sciencesignaling.org/cgi/content/full/3/153/ra90/DC1

Supplementary Materials for

The Mammalian MAPK/ERK Pathway Exhibits Properties of a Negative Feedback Amplifier

Oliver E. Sturm, Richard Orton, Joan Grindlay, Marc Birtwistle, Vladislav Vyshemirsky, David Gilbert, Muffy Calder, Andrew Pitt, Boris Kholodenko, Walter Kolch*

*To whom correspondence should be addressed. E-mail: walter.kolch@ucd.ie

Published 21 December 2010, *Sci. Signal.* **3**, ra90 (2010)
DOI: 10.1126/scisignal.2001212

This PDF file includes:

Other Supplementary Material for this manuscript includes the following:
(available at www.sciencesignaling.org/cgi/content/full/3/153/ra90/DC1)

Supplementary Sections 1-3, References, and Figures

Section 1. Models and Modelling

The mathematical models were based on mass action models using ordinary differential equations. We constructed two computational models, Feedback Intact and Feedback Broken, to investigate the negative feedback amplifier (NFA) characteristics of the extracellular signal-regulated protein kinase (ERK) pathway. These computational models were based on the core ERK pathway of the Schoeberl *et al*. model *(1)* and, therefore, utilize ordinary differential equations (ODEs).

1.1: Feedback Intact Model and Amplifier Perturbation

The Feedback Intact model (fig. S2A) starts at the level of Ras, ends at the level of ERK, and includes a negative feedback loop from activated ERK to both active and inactive Raf-1 executed by direct inhibitory phosphorylation of Raf-1 by ERK *(2)*. Because activation of Ras is the key obligatory event for Raf-1 activation by different receptor tyrosine kinases *(3-5)*, we used Ras activity (measured by the abundance of RasGTP) as a surrogate for receptor activity in the model. This means that the Feedback Intact model is focussed on the core ERK pathway, which is essentially the NFA module of interest. A table of reactions, species, and kinetic parameters for the Feedback Intact model is presented in the Model_Intact (table S1).

We used the specific MEK Inhibitor U0126 *(6)* to perturb the amplifier module. U1026 was originally characterized as a noncompetitive or mixed inhibitor *(7)*. Detailed enzyme

kinetic studies showed that U0126 does not prevent the activating phosphorylation of MEK by Raf kinases, but blocks binding and phosphorylation of the ERK substrate *(8)*. Structural studies suggest that MEK inhibitors interact with the substrate-binding domain of MEK and may lock MEK in an inactive conformation *(9)*. Thus, in the model, U0126 is represented as allosteric inhibitor, which can bind to all forms of MEK and does not interfere with the activation of MEK by Raf or the deactivation of MEK by its phosphatase.

In theory, the Feedback Intact model should behave similarly to a NFA because it has a constant input, an amplifier module, a constant output, and negative feedback loops. Therefore, the system should resist the effects of a MEK inhibitor, such as U0126. We employed the following strategy to investigate the resistance of the system to U0126, and, therefore, the NFA characteristics of the ERK pathway. Initially, the model has no U0126 present and is simulated for 3,600,000,000 seconds to reach a steady state, at which time the concentration of total activated ERK (ppERK) is obtained; total ppERK corresponds to all ppERK-containing species in the model and is used to compare to the Western blot laboratory data. Then, a new simulation is run, starting from the same initial conditions as before except in the presence of a low concentration of U0126; again, the model is simulated for 3,600,000,000 seconds to reach a steady state and the final concentration of total ppERK is obtained (simulations were examined to check that a steady state had been achieved). The initial concentration of U0126 is increased incrementally from 0, with a new simulation run at each increment stage and with the final concentration of total ppERK obtained for each simulation run. Plotting the initial concentration of U0126 against the final total concentration of ppERK for each simulation run reveals how the system responds to an increasing disturbance caused by U0126. We used the Scan function of the pathway simulation tool Gepasi (Mendes, 1999; www.gepasi.org) to create the graph. The Feedback Intact system i resists the effects of U0126 and maintain relatively high abundances of ppERK over a broad inhibitor concentration range (Fig. 3C).

1.2: Feedback Broken Model

The Feedback Broken model starts at BXB-ER and ends at ERK (fig. S2B). BXB-ER is an artificial fusion protein in which the kinase domain of Raf-1 is fused to the hormone-binding domain of the estrogen receptor *(10)*. The kinase activity of BXB-ER is independent of Ras activity and instead can be acutely regulated by the synthetic estrogen analog 4-hydroxy-tamoxifen (4HT) with activation kinetics similar to those of endogenous Raf-1 *(10, 11)* (Fig. 1F). BXB-ER lacks five of the six ERK feedback phosphorylation sites (fig. S3) and is completely resistant to negative feedback regulation by ERK (Fig. 1F). Therefore, this model lacks any negative feedback loops because activation of ERK through BXB-ER lacks both the ERK negative feedback loop to Raf-1 and to SOS and, thus, to Ras activation. The MEK inhibitor U0126 is incorporated in this model as described above. A table of reactions, species, and kinetic parameters for the Feedback Broken model is presented in the Broken_Model (table S2).

In theory, the Feedback Broken model should behave as a standard amplifier, and the system should be sensitive to even low concentrations of an amplifier inhibitor, such as U0126. The strategy to investigate the resistance of the system to U0126 was the same as described above for the Feedback Intact model. The results show that the Feedback Broken model is inhibited at low concentrations of U0126; whereas the Feedback Intact model is much more resistant to inhibition of the amplifier with ppERK abundance remaining relatively high over a broad concentration range.

1.3: Input Strengths Selection, Parameter Values, and Comparison Between Feedback Intact and Broken Models

To directly compare the relationship between input strength and dose response of the two models, they need to have comparable input strengths. The Feedback Broken model has BXB-ER as input, whereas the Feedback Intact model has RasGTP as input. For the purposes of comparing input dose and inhibition responses between the Feedback Broken and Feedback Intact models, we modified the Feedback Broken model with a pseudo-input S, which acts like RasGTP in the Intact model. We normalized the steady-state input and output relationships by the value of input (RasGTP or BXB-ER), which produced half-maximal ERK activation (Fig. M1). We also compared how the Feedback Broken and Intact models responded to input inhibition (Fig. M1). Although the Feedback Broken model resists input inhibition better than the Feedback Intact model at less than half-maximal inhibition, it displays catastrophic failure around half-maximal inhibition. This catastrophic failure is not observed with the Feedback Intact model, where ppERK abundances smoothly decline with increasing input inhibition. These results thus imply that the negative feedback provides robustness to input perturbations.

To determine appropriate input strengths to use in further simulations, we examined the input/output relationship of the model by scanning through the initial concentration of BXB-ER as input and monitoring the steady-state concentration of total ppERK as output. We selected an input strength of 4,000 BXB-ER molecules for the Feedback Broken model, because this was near the center of the input/output response curve (Fig. M1). For the Feedback Intact model, the input strength was consequently set to the concentration of RasGTP as input that yielded a total of approximately 4,000 activated Raf-1 molecules, which was comparable to the 4,000 BXB-ER molecules. Input/output analyses determined that this concentration was 5,350 RasGTP molecules (Fig. M1. Thus, the two models have equal input strengths, which have been normalized to the abundance of active Raf-1 molecules in the system. We also calibrated the Raf input experimentally by titrating 4HT to give BXB-ER activation strength and kinetics similar to those of EGF-activated endogenous Raf-1 (Fig. 1F). In the experiments with the Raf6A mutant, for the control we used cells that were transfected with wild-type Raf-1 expressed at similar abundance to that in cells expressing the Raf6A mutant (fig. S4). Thus, we can make reliable comparisons of the responses of the different (biological and computational) model systems to drug perturbations.

Our models are normalized to the Raf input strength, but other parameters were not adjusted to make the models equivalent. We explored how parameter changes affected

the responses to U1026 inhibition by comparing the Feedback Intact and Feedback Broken models (Fig. M2) in simulations in which each kinetic parameter, in both models (intact and broken), was sampled from a uniform distribution +/- 1 order of magnitude from its nominal value. We ran 1000 different steady-state simulations for every value of U0126, each with a different realization of the kinetic parameters. With 10 different U0126 concentrations, this corresponds to 10,000 parameter sets. The results show that even under these widely varying parameter conditions the shape of the response curves in both models stays essentially the same (fig. M2).

1.4: EGFR Inhibitor

Because the amplifier is located within the negative feedback loop, NFAs compensate for disturbances to the amplifier and, therefore, maintain relatively stable output strengths. However, NFAs do not compensate for disturbances to the input, because the input is located outside of the negative feedback loop. Applying this to the biological situation implies that drugs, like U0126, that target components embedded within the negative feedback loop will be less effective than drugs targeting components outside of the feedback amplifier module. An example of such a drug is the EGF receptor (EGFR) inhibitor 4557W, which binds to the EGFR and blocks its kinase activity *(12)*. Therefore, 4557W decreases the number of receptors that can activate the downstream ERK pathway and interferes with the input into the negative feedback amplifier, for which the system should be unable to compensate.

Because the Feedback Intact model starts at the level of RasGTP, rather than the EGFR itself, the effects of 4557W cannot be modelled directly. However, the effects of 4557W on the input into the NFA module can be investigated within a qualitative, core model, where the effect of decreasing the number of activated EGFR is modelled as a decrease in the initial RasGTP abundance. Technically, this was accomplished with the Scan function of Gepasi.

1.5: Sensitivity Analysis

Sensitivity analysis is a commonly used approach to study the response of system variables to changes in parameter values and can therefore be used to identify the key reactions and species in a model *(13)*. Furthermore, sensitivity analysis can also be used to assess the robustness of a model. Sensitivity analysis works by varying a parameter value by a small amount and analyzing what effect this has on a specific system variable, for example, the steady-state concentration of total ppERK. A small change to a key parameter value is likely to have a large effect on the system variable. It is important to note that different parameters can have widely different sensitivities, and the sensitivity of a specific parameter can also vary depending on which system variable is considered. The sensitivity coefficient (SC) of a specific parameter P with respect to a specific system variable V can be calculated using Equation 1; δV represents the change in the system variable V due to the change in the parameter P (δP).

$$SC_P^V = \frac{\delta V / V}{\delta P / P}$$

Equation 1. *Sensitivity Coefficient (SC) equation of parameter P with respect to system variable V.*

We performed sensitivity analysis to compare how robust the Feedback Intact and Feedback Broken models were in the absence of inhibitors (Fig. 2B). We individually varied every kinetic rate constant +10% in each of the two models and monitored the effect of each variation on total steady state abundances of ppERK and then calculated a sensitivity coefficient for each rate constant using Equation 1. We also varied each kinetic rate constant by -10% and calculated another sensitivity coefficient for each rate constant. The two sensitivity coefficients were then averaged to give a single sensitivity coefficient for every rate constant in each of the two models. As the Feedback Intact and Feedback Broken models share a large number of identical reactions, and therefore parameters, sensitivity coefficients can be directly compared to one another enabling the robustness of the models to be compared.

1.6: Non Steady-State Responses

We assessed the transient behavior of the system to further analyze the NFA characteristics of the ERK pathway. We stimulated the system and then, when ppERK abundances reached their maximum, we introduced the MEK inhibitor U0126, and monitored ppERK abundances over time to examine how the system responds to this disturbance. In theory, when the feedback loop is intact the system should recover from the disturbance caused by U0126 and ppERK abundances should increase reaching a new equilibrium. Whereas, when the feedback loop is broken, the system should fail to compensate for the disturbance caused by U0126 and ppERK abundances should not recover.

This investigation was performed as follows. First, we created a Feedback Intact model that contained no U0126 and no U0126 reactions. This model was simulated for 360 seconds (6 minutes) at which point ppERK abundances are at their maximum. Second, the final concentrations of all the species from this initial simulation were transferred to a new Feedback Intact model that did contain U0126 (10,000,000 molecules) and U0126 reactions. This means that the new U0126 model starts off from exactly the same position that the first non-U0126 model finished. Third, this U0126 model was then simulated for 3240 seconds (54 minutes) and the two simulation results were combined to give a 3600 second (1 hour) time course where U0126 was added at the peak of ERK activation (Fig.S6A). The same strategy was used for the Feedback Broken model, except that the concentration of BXB-ER (the input) was increased to 6,416 molecules for this simulation so that ppERK abundances for the two models were approximately the same at the point where U0126 was added Experimentally, these predictions were tested by adding U0126 at the peak of ERK activation (Fig. S6B). The results are consistent with the model predictions that the NFA will cause the system to recover at a higher activity

than the basal state, which is not possible without the negative feedback. The exact kinetics between the simulation and the experimental result are different, but this is not surprising because the effects of the inhibitor in the model are immediate, whereas in the experimental situation the inhibitor has to diffuse into the cell and accumulate to effective inhibitory concentrations.

1.7: The Effects of B-Raf

The Feedback Intact model included a single Raf isoform, Raf-1, and ignored B-Raf. We did not consider B-Raf initially because the COS1 cell line that we used does not have detectable amounts of B-Raf *(14)*. However, most cells have both Raf-1 and B-Raf *(15)*. In addition, B-Raf and Raf-1 heterodimerize *(16-18)*, and oncogenic B-Raf mutants with low kinase activity were reported to need Raf-1 to efficiently activate ERK *(16)*. The B-Raf/Raf-1 heterodimer has very high kinase activity towards MEK, although it is only formed at low stoichiometry *(17)*. The formation of the B-Raf/Raf-1 heterodimer is mitogenic and induced by active Ras *(16-18)*. The lifetime of the dimer, but not its formation, is subjected to a negative feedback by ERK *(17, 19)*. The kinase activity of B-Raf is not susceptible to negative feedback regulation by ERK (Fig. S8).

These data suggest that B-Raf does not participate in the NFA. However, Raf-1 and B-Raf compete with each other for activation by RasGTP. This competition could possibly interfere with the NFA properties because the abundances of active B-Raf could decrease due to increased competition from Raf-1 when the negative feedback loop is weakened after drug treatment. This would mean that the overall abundances of active Raf species remains relatively constant, whereas increasing abundances of active Raf are needed to display NFA behavior. Therefore, we created the B-Raf Feedback Intact model in which the Feedback Intact model was expanded to include B-Raf (table S3) and to investigate the effect of B-Raf on the system's ability to behave as a NFA and resist the effects of the MEK inhibitor U0126. The presence of B-Raf did not eliminate the NFA characteristic that allowed the system to resist the effects of U0126 and to maintain relatively high abundances of ppERK over a broad range of U1026 concentrations (fig. M3), similar to the simulations of the Feedback Intact model (Fig. 3C). The simulations also showed that the abundances of active B-Raf remained relatively stable as the concentration of U0126 increased, whereas the abundances of active Raf-1 increased due to a weakening of the negative feedback loop from ERK to Raf-1 (fig. M4). Furthermore, assigning distinct phosphatases to Raf-1 and B-Raf to eliminate competition for deactivation had little effect (fig. M5). Therefore, these results suggest that B-Raf does not change the NFA characteristics of the ERK cascade and does not interfere with the system's ability to resist inhibition by U0126. A table of reactions, species, and kinetic parameters for the B-Raf Feedback Intact model is presented in the Model_B-Raf (table S3).

1.8: Computational Tools

We used Gepasi *(20)* (www.gepasi.org) as the computational tool for model construction, simulation, and analysis. We used the SimBiology toolbox of Matlab

(http://www.mathworks.com) to double-check the simulation results obtained from Gepasi.

Section 1 figures M1-M5

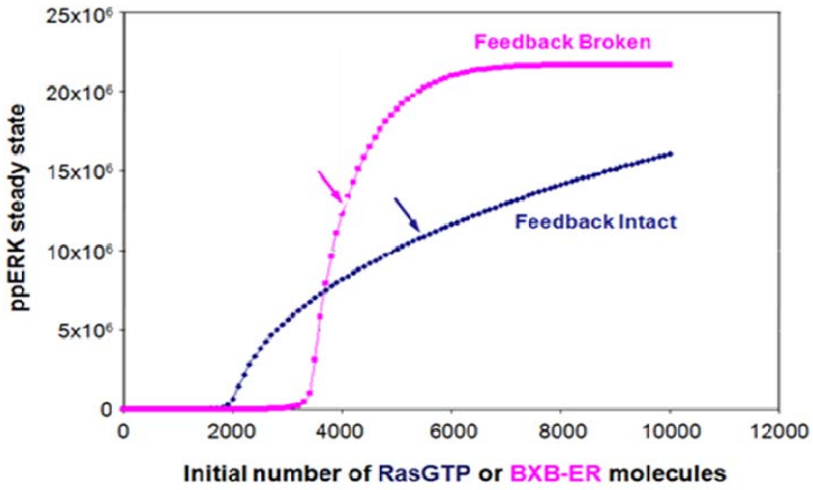

Fig. M1. ERK-PP input/output response curves of the Feedback Intact and Feedback Broken models. *The x-axis represents the input level which corresponds to initial BXB-ER molecules for the Feedback Broken model and initial RasGTP molecules for the Feedback Intact model; the y-axis represents total steady state [ERK-PP]. For each model, an arrow points to the input level that was selected and used for further investigations of the effects of the MEK inhibitor U0126 and for sensitivity analyses. The two arrows are not located at exactly the same point on the input x-axis because the input levels were selected based on normalisation at the level of active Raf whereas the x-axis corresponds to two different inputs (RasGTP & BXB-ER). However, both arrows are still in the centre of their corresponding response curves which means the two models are in a comparable state.*

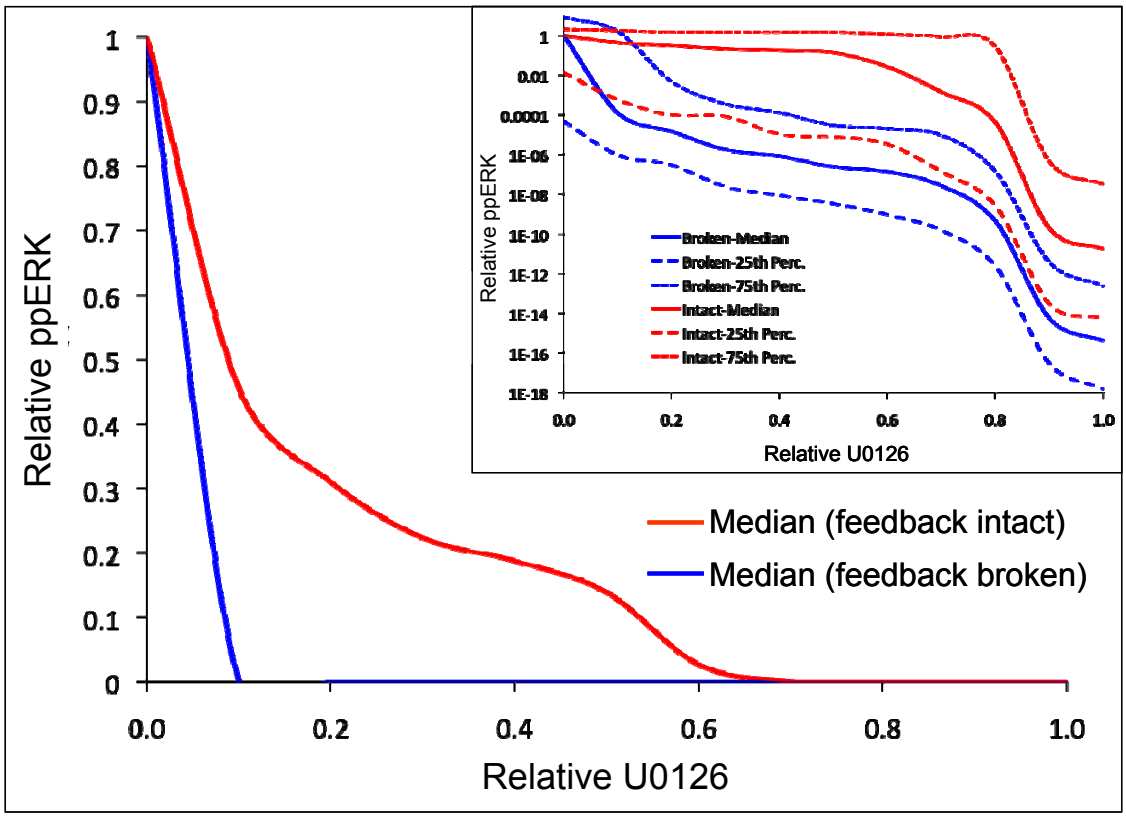

Fig. M2. Effects of parameter variations in the Feedback Broken and Feedback Intact models. *Parameters spanning +/- 1 order of magnitude from the nominal value were sampled in simulations with the various concentrations of U1026 as described in section 1.3. The medians of steady-state ppERK concentrations are plotted. The inset shows the median of the steady-state ppERK abundances along with the 25th and 75th percentiles. Note that the inset y-axis is on a log scale to assure that all curves are visible on the plot.*

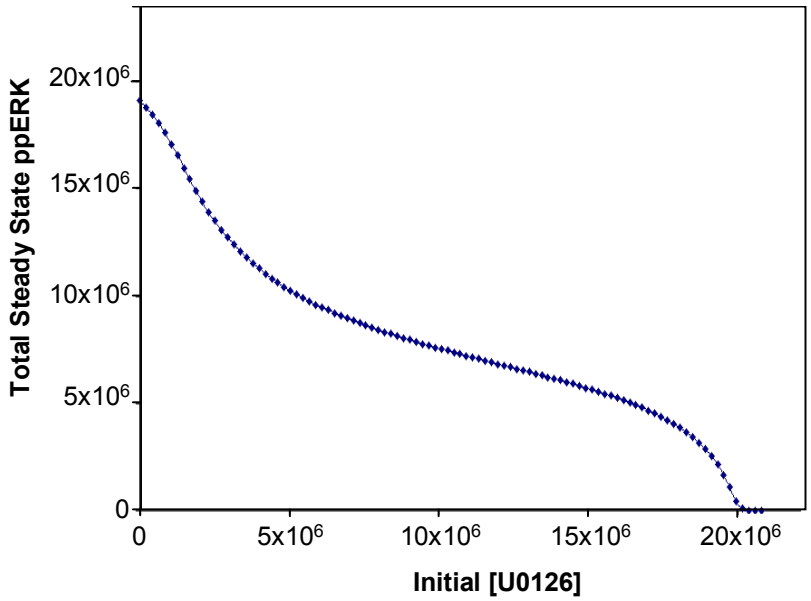

Fig. M3. ppERK response of the B-Raf Feedback Intact model to an increasing initial concentration of U0126. *This graph displays the steady-state concentration of total ppERK (y-axis) after different initial concentrations of U0126 (x-axis) given as number of molecules for the B-Raf Feedback Intact model.*

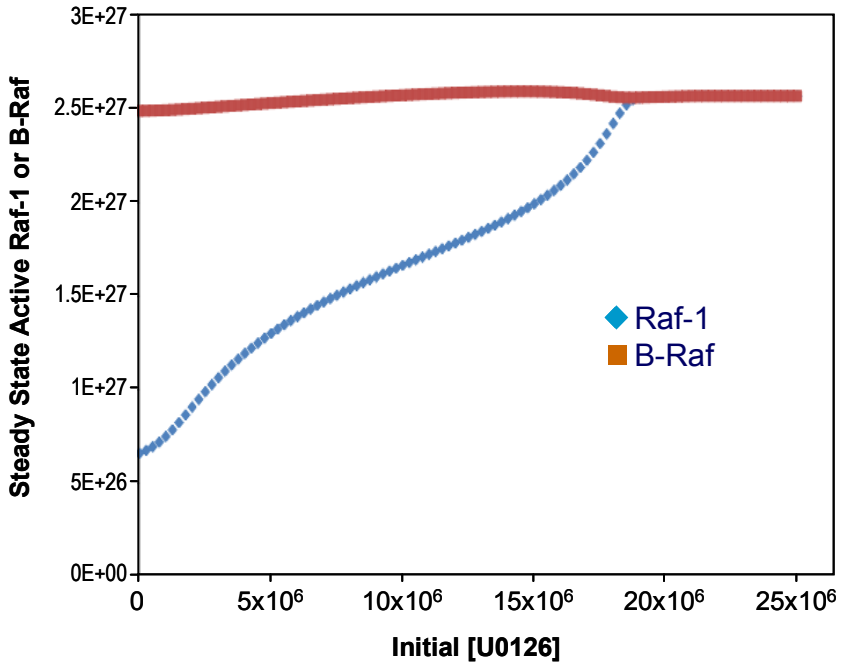

Fig. M4. Active Raf-1 and B-Raf steady-state response to an increasing initial concentration of U0126. *This graph displays the steady-state concentration of total active Raf-1 or B-Raf (y-axis) after different initial concentrations of U0126 (x-axis) for the B-Raf Feedback Intact model.*

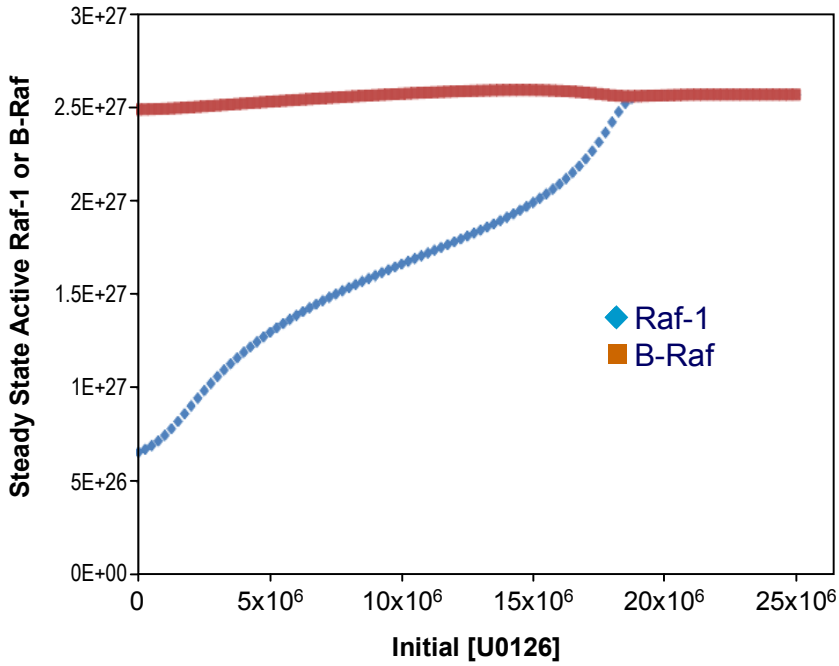

Fig. M5. Active Raf-1 and B-Raf steady-state response to an increasing initial concentration of U0126 when Raf-1 and B-Raf are deactivated by different phosphatises. *This graph displays the steady-state concentration of total active Raf-1 or B-Raf (y-axis) after different initial concentrations of U0126 (x-axis) for the B-Raf Feedback Intact model when separate phosphatases of equal abundance deactivate Raf-1 and B-Raf.*

Section 2. Model Parameters

The parameters for each model are presented in a single Excel file with an individual worksheet for table S1-3 of model parameters. The parameters include the forward and reverse rate constants, the rate number assigned to each rate constant, the units of the rate constants, and the starting amounts for each of the molecules, along with the sources upon which the parameters are based.

Table S1. Model_Intact in the Excel file corresponds to the Feedback Intact model.
Table S2. Model_Broken in the Excel file corresponds to the Feedback Broken model.
Table S3. Model_B-Raf in the Excel file corresponds to the Feedback Intact model in which the Feedback Intact model has been expanded to include B-Raf.

Section. 3. SBML Files of the Models

Systems Biology Markup Language (SBML; www.sbml.org) files of the models are provided.

References

1. B. Schoeberl, C. Eichler-Jonsson, E. D. Gilles, G. Muller, Computational modeling of the dynamics of the MAP kinase cascade activated by surface and internalized EGF receptors. *Nat Biotechnol* **20**, 370 (2002).
2. M. K. Dougherty, J. Muller, D. A. Ritt, M. Zhou, X. Z. Zhou, T. D. Copeland, T. P. Conrads, T. D. Veenstra, K. P. Lu, D. K. Morrison, Regulation of Raf-1 by direct feedback phosphorylation. *Mol Cell* **17**, 215 (2005).
3. A. S. Dhillon, W. Kolch, Untying the regulation of the Raf-1 kinase. *Arch Biochem Biophys* **404**, 3 (2002).
4. W. Kolch, Coordinating ERK/MAPK signalling through scaffolds and inhibitors. *Nat Rev Mol Cell Biol* **6**, 827 (2005).
5. C. Wellbrock, M. Karasarides, R. Marais, The RAF proteins take centre stage. *Nat Rev Mol Cell Biol* **5**, 875 (2004).
6. J. Urosevic, E. Y. Sum, V. Moneo, M. Drosten, A. Dhawahir, M. Becerra, A. Carnero, M. Barbacid, Using cells devoid of RAS proteins as tools for drug discovery. *Mol Carcinog* **48**, 1038 (2009).
7. M. F. Favata, K. Y. Horiuchi, E. J. Manos, A. J. Daulerio, D. A. Stradley, W. S. Feeser, D. E. Van Dyk, W. J. Pitts, R. A. Earl, F. Hobbs, R. A. Copeland, R. L. Magolda, P. A. Scherle, J. M. Trzaskos, Identification of a novel inhibitor of mitogen-activated protein kinase kinase. *J Biol Chem* **273**, 18623 (1998).
8. W. S. VanScyoc, G. A. Holdgate, J. E. Sullivan, W. H. Ward, Enzyme kinetics and binding studies on inhibitors of MEK protein kinase. *Biochemistry* **47**, 5017 (2008).
9. J. F. Ohren, H. Chen, A. Pavlovsky, C. Whitehead, E. Zhang, P. Kuffa, C. Yan, P. McConnell, C. Spessard, C. Banotai, W. T. Mueller, A. Delaney, C. Omer, J. Sebolt-Leopold, D. T. Dudley, I. K. Leung, C. Flamme, J. Warmus, M. Kaufman, S. Barrett, H. Tecle, C. A. Hasemann, Structures of human MAP kinase kinase 1 (MEK1) and MEK2 describe novel noncompetitive kinase inhibition. *Nat Struct Mol Biol* **11**, 1192 (2004).
10. M. L. Samuels, M. J. Weber, J. M. Bishop, M. McMahon, Conditional transformation of cells and rapid activation of the mitogen-activated protein kinase cascade by an estradiol-dependent human raf-1 protein kinase. *Mol Cell Biol* **13**, 6241 (1993).
11. J. Lovric, S. Dammeier, A. Kieser, H. Mischak, W. Kolch, Activated raf induces the hyperphosphorylation of stathmin and the reorganization of the microtubule network. *J Biol Chem* **273**, 22848 (1998).

12. S. Cockerill, C. Stubberfield, J. Stables, M. Carter, S. Guntrip, K. Smith, S. McKeown, R. Shaw, P. Topley, L. Thomsen, K. Affleck, A. Jowett, D. Hayes, M. Willson, P. Woollard, D. Spalding, Indazolylamino quinazolines and pyridopyrimidines as inhibitors of the EGFr and C-erbB-2. *Bioorg Med Chem Lett* **11**, 1401 (2001).
13. H. Kacser, J. A. Burns, The control of flux. *Symp Soc Exp Biol* **27**, 65 (1973).
14. E. M. Weissinger, G. Eissner, C. Grammer, S. Fackler, B. Haefner, L. S. Yoon, K. S. Lu, A. Bazarov, J. M. Sedivy, H. Mischak, W. Kolch, Inhibition of the Raf-1 kinase by cyclic AMP agonists causes apoptosis of v-abl-transformed cells. *Mol Cell Biol* **17**, 3229 (1997).
15. G. Galabova-Kovacs, A. Kolbus, D. Matzen, K. Meissl, D. Piazzolla, C. Rubiolo, K. Steinitz, M. Baccarini, ERK and beyond: insights from B-Raf and Raf-1 conditional knockouts. *Cell Cycle* **5**, 1514 (2006).
16. M. J. Garnett, S. Rana, H. Paterson, D. Barford, R. Marais, Wild-type and mutant B-RAF activate C-RAF through distinct mechanisms involving heterodimerization. *Mol Cell* **20**, 963 (2005).
17. L. K. Rushworth, A. D. Hindley, E. O'Neill, W. Kolch, Regulation and role of Raf-1/B-Raf heterodimerization. *Mol Cell Biol* **26**, 2262 (2006).
18. C. K. Weber, J. R. Slupsky, H. A. Kalmes, U. R. Rapp, Active Ras induces heterodimerization of cRaf and BRaf. *Cancer Res* **61**, 3595 (2001).
19. T. Brummer, H. Naegele, M. Reth, Y. Misawa, Identification of novel ERK-mediated feedback phosphorylation sites at the C-terminus of B-Raf. *Oncogene* **22**, 8823 (2003).
20. P. Mendes, GEPASI: a software package for modelling the dynamics, steady states and control of biochemical and other systems. *Comput Appl Biosci* **9**, 563 (1993).

Supplementary Figure S1

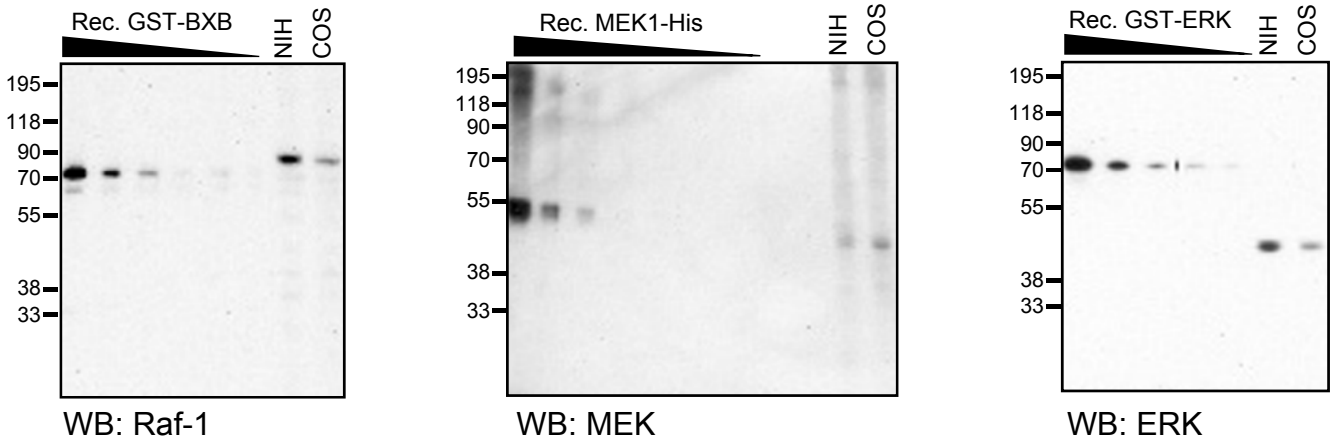

Cell line	Raf-1	MEK	ERK	Amount per cell
COS1	3.6	10.6	21.2	attomol (10^{-18})
	1	2.9	5.9	ratio
NIH 3T3	10.9	7.1	98	attomol (10^{-18})
	1	0.7	9	ratio

Fig. S1. Absolute concentrations of Raf-1, MEK, and ERK in COS1 and NIH 3T3 cells. Recombinant proteins representing the Raf-1 kinase domain (GST-BXB), MEK1 (MEK1-His) and ERK2 (GST-ERK) were expressed in E.coli and purified to >80% homogeneity as judged by Coomassie staining. These recombinant protein were used as standards to determine the concentrations of the respective proteins in lysates of NIH/3T3 and COS1 cells. To estimate molar concentrations per cell, an average cell volume of 5pL was used.

Supplementary Figure S2

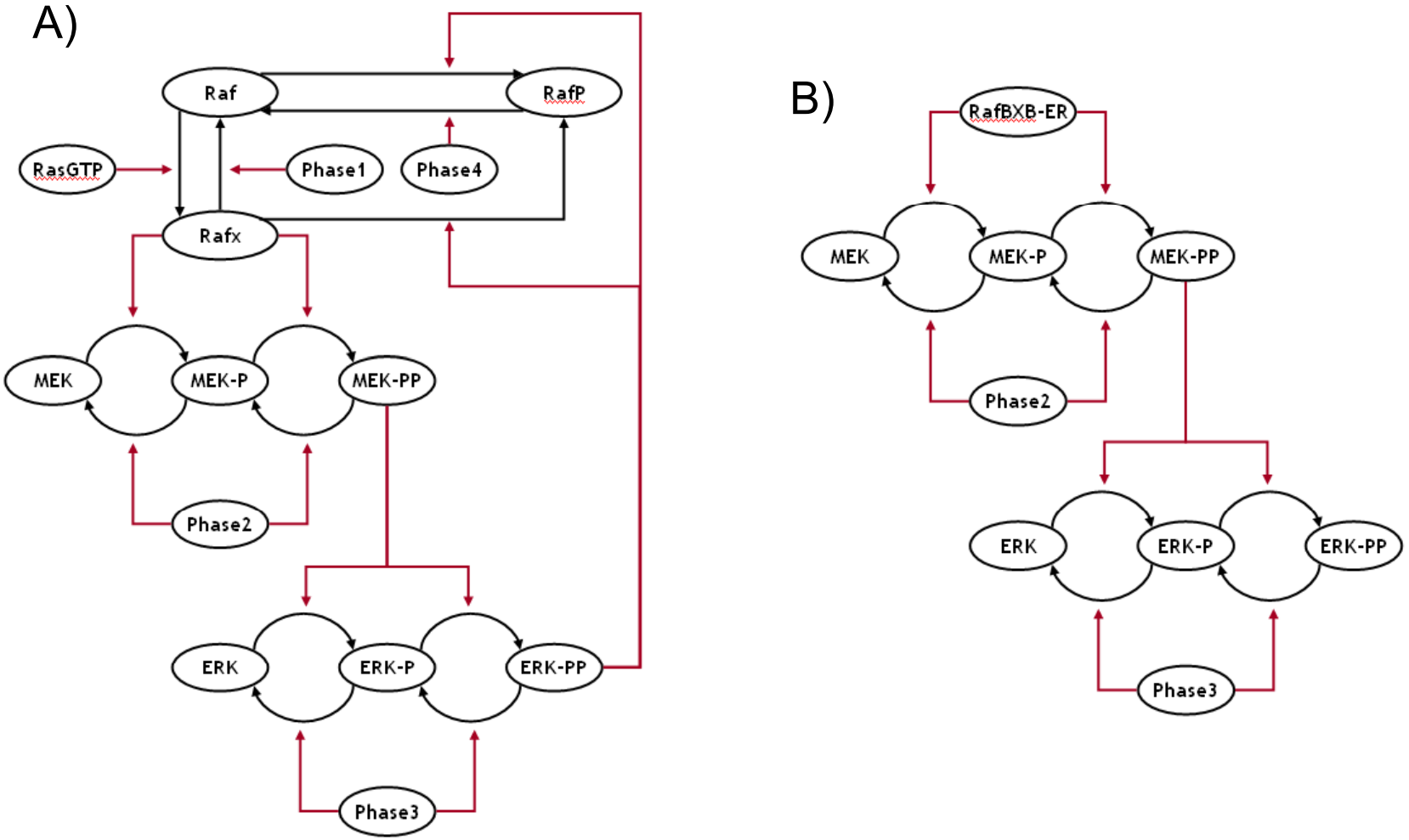

Fig. S2. Schematic topologies of the models used. (A) The Feedback Intact model starts at the level of RasGTP and ends at the level of ERK. It includes a negative feedback loop from activated ERK to both active and inactive Raf. Rafx, activated Raf; RafP, Raf deactivated by ERK feedback phosphorylation; Phase, phosphatase; MEK-P, ERK-P and MEK-PP, ERK-PP, single and double phosphorylated MEK and ERK, respectively. **(B)** The Feedback Broken model starts at the level of RafBXB-ER, ends at the level of ERK and does not include a negative feedback loop.

Supplementary Figure S3

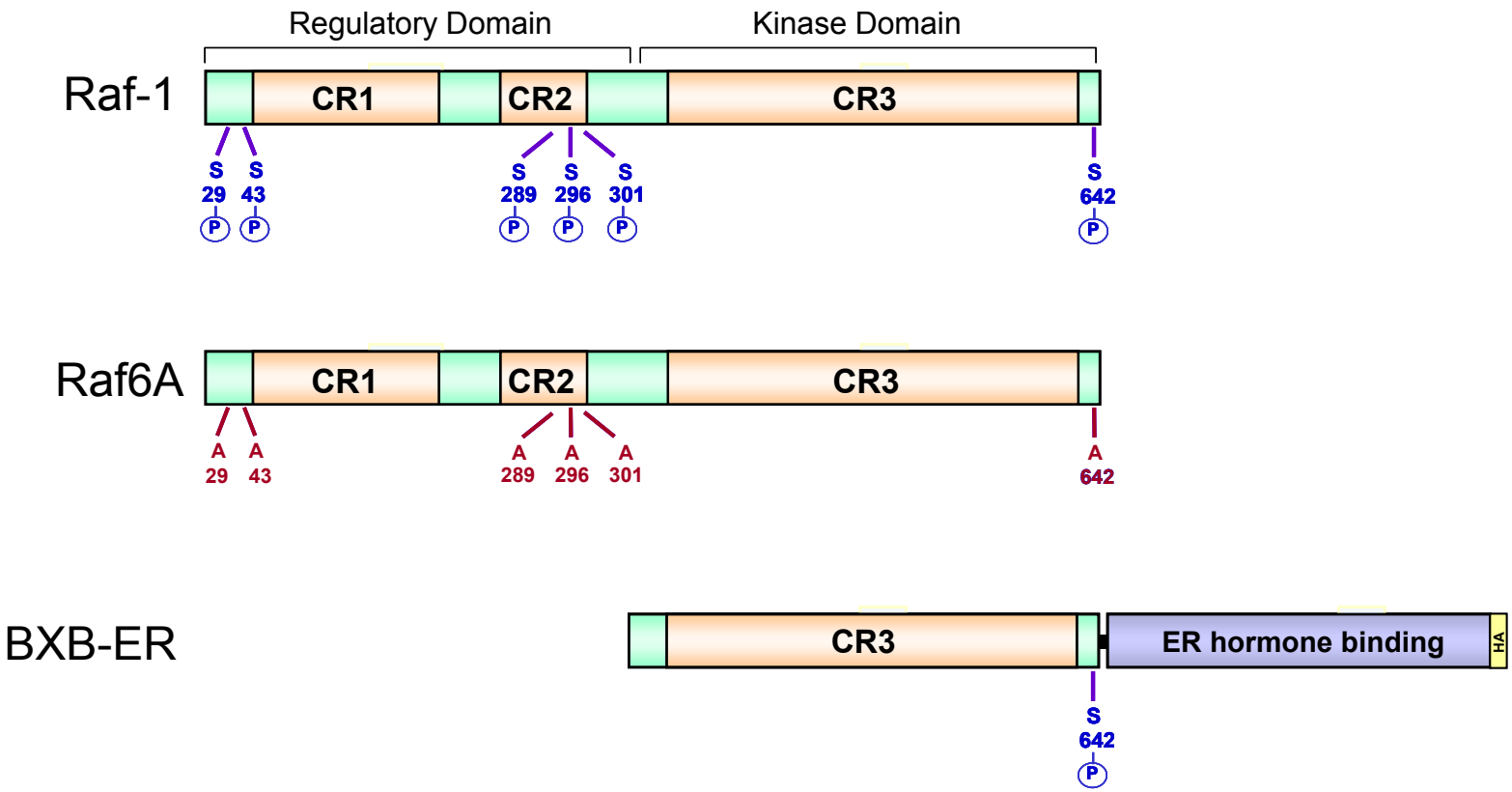

Fig. S3. Schematic of Raf-1 and the Raf-1 mutants used to probe the NFA hypothesis.
Inhibitory ERK phosphorylation sites as mapped by Dougherty et al. Mol Cell 17, 215-224 (2005) are indicated. In the Raf-1 6A mutant (a kind gift from D. Morrison) these serines are replaced by alanines. BXB-ER contains the Raf-1 kinase domain fused to the hormone binding domain of the estrogen receptor (ER). For ease of detection and isolation an HA-tag was added to the C-terminus (Lovric et al., J Biol Chem. 273, 22848-22855, 1998). CR; conserved region.

Supplementary Figure S4

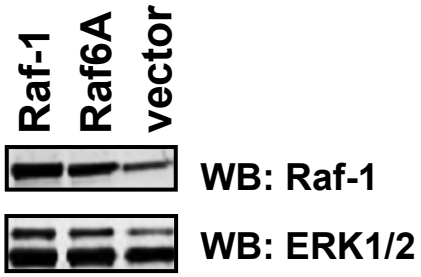

Fig. S4. Expression of Flag-tagged Raf-1 and the Raf6A mutant were tested by Western blotting with a Raf-1 specific antibody. ERK1/2 expression was used as loading control.

Supplementary Figure S5

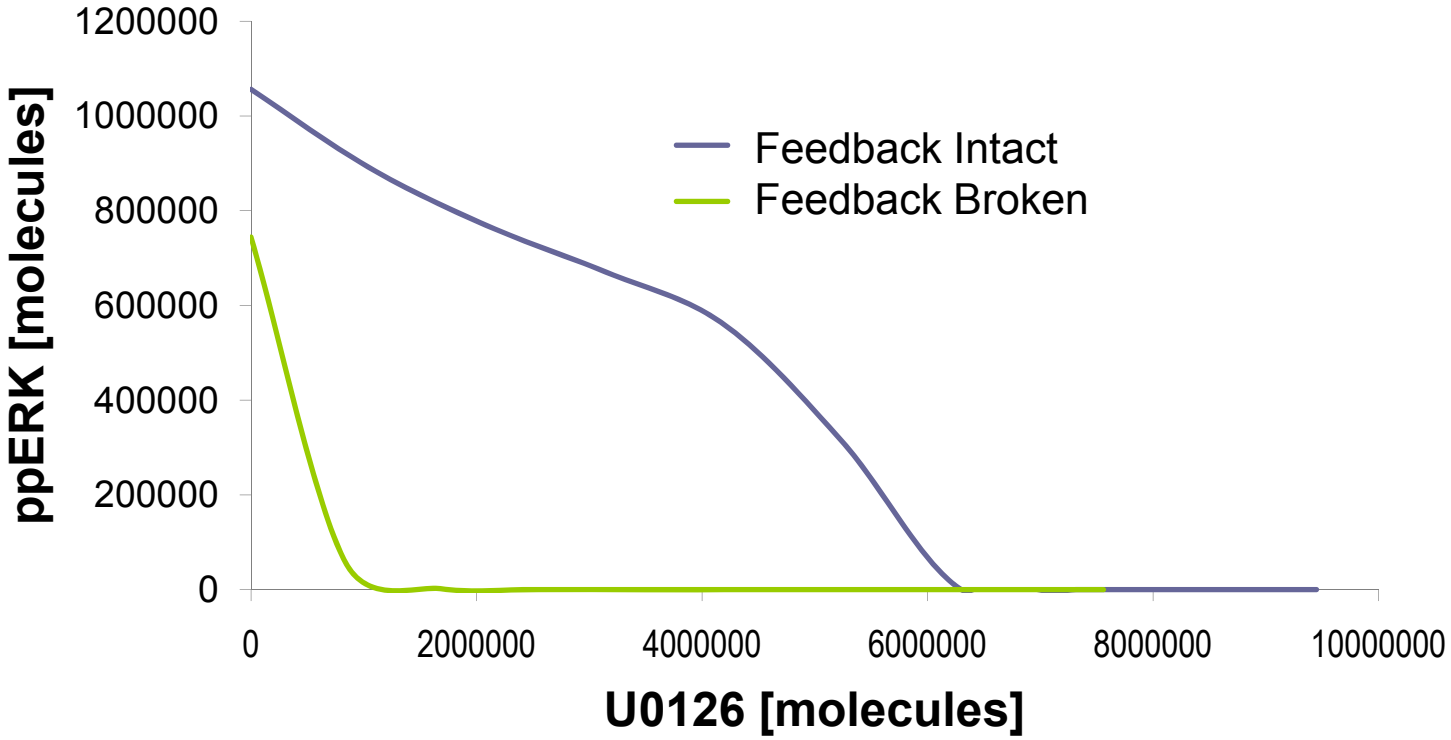

Fig. S5. The effects of U0126 on steady-state ppERK abundance with protein concentrations of COS1 cells. Total protein concentrations as determined in fig. S1 for COS1 cells were taken as (in molecules/cell): Raf-1 (2 million), MEK (6 million), ERK (12 million). For the Feedback Intact model, the RasGTP input was set to 2500 molecules/cell, whereas for the Feedback Broken model, the active Raf input was set to 4800 molecules/cell.

Supplementary Figure S6

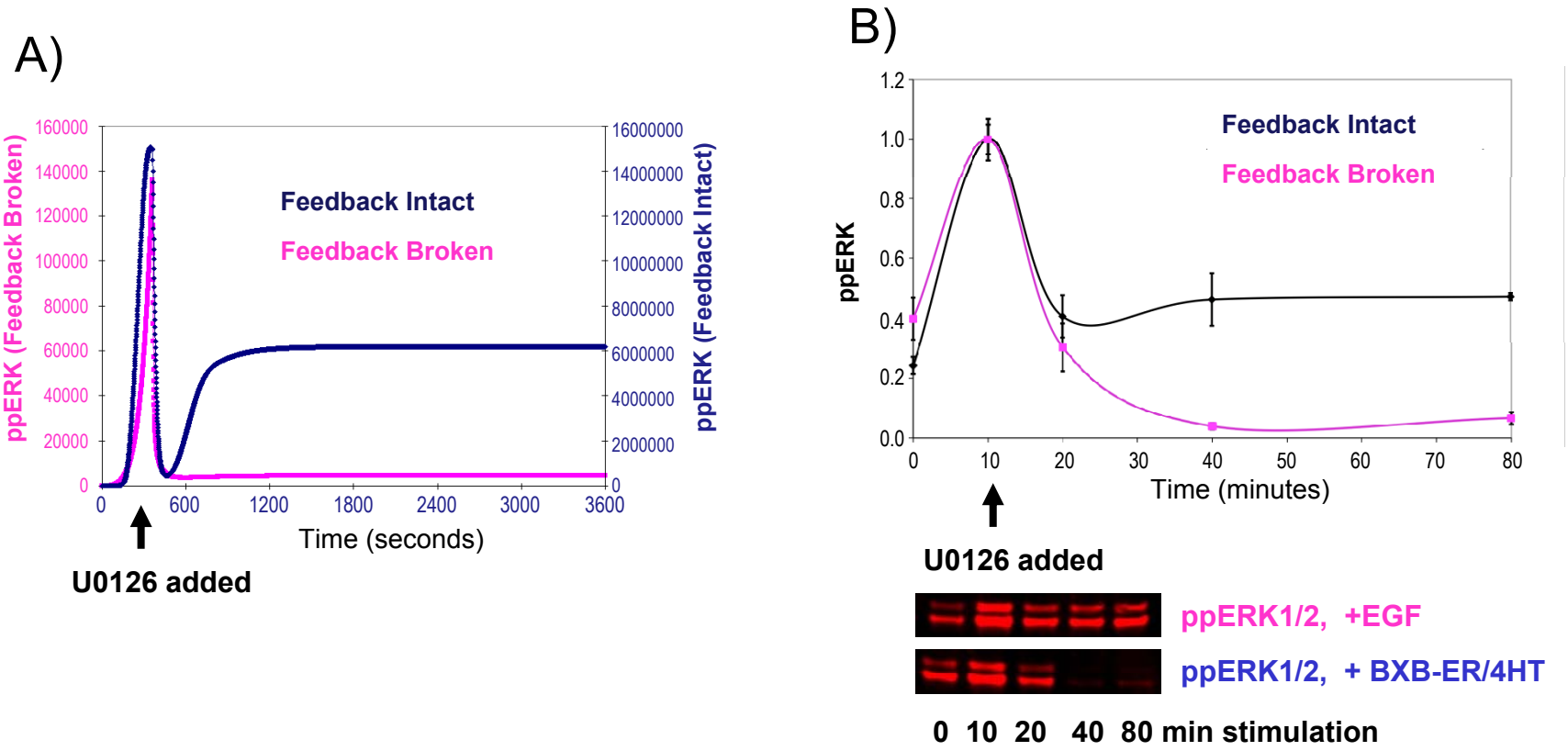

Fig. S6. The NFA effect also stabilizes non-steady-state dynamic systems.
(A) Simulation of adding U0126 at the peak of ERK activation. **(B)** Experimental results of adding U0126 at the peak of ERK activation. A stable BXB-ER COS1 cell line was stimulated with EGF or 4-Hydroxy-tamoxifen (4HT). In both cases, 1 μM of U0126 was added 10 minutes after treatment with EGF or 4HT. ERK activity was measured by LICOR.

Supplementary Figure S7

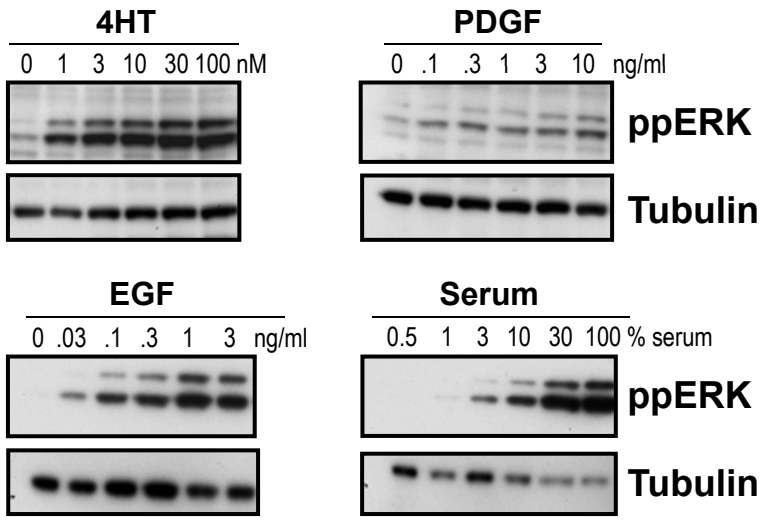

Fig. S7. Dose-dependent ERK activation by different stimuli. NIH/3T3 cells stably expressing BXB-ER(*31*) were stimulated with increasing amounts of 4-hydroxy-tamoxifen (4HT), platelet derived growth factor (PDGF), epidermal growth factor (EGF), or foetal calf serum (serum). ERK phosphorylation (ppERK) was determined by Western blotting. Tubulin was used loading control.

Supplementary Figure S8

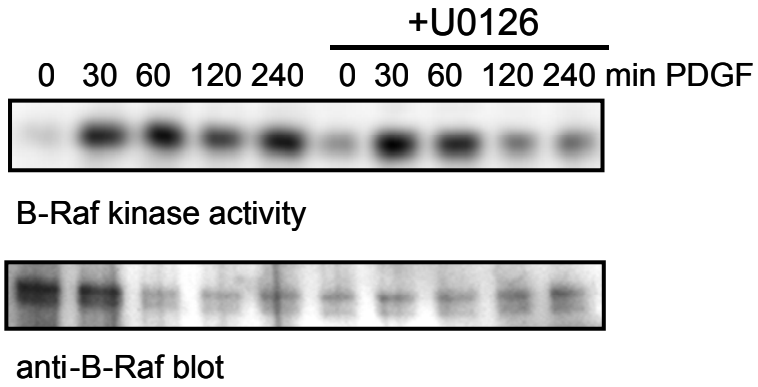

Fig. S8. B-Raf kinase activity is not feedback-inhibited by ERK. Endogenous B-Raf was immunoprecipitated from cells treated with 50ng/ml PDGF for the indicated time points. B-Raf kinase activity was measured as described (Rushworth et al. Mol Cell Biol 26, 2262-2272 2006) using GST-MEK as substrate.